# Correlation between the structural and transport properties of as-grown epitaxial phase-separated Co-Ag thin films

K. Ounadjela
*Institut de Physique et Chimie des Matériaux de Strasbourg, CNRS, 23 Rue du Loess, 67037 Strasbourg, France*

S. M. Thompson
*Department of Physics, University of York, Heslington, York, YO1 5DD, United Kingdom*

J. F. Gregg
*Clarendon Laboratory, University of Oxford, Parks Road, Oxford, OX1 3PU, United Kingdom*

A. Azizi, M. Gester, and J. P. Deville
*Institut de Physique et Chimie des Matériaux de Strasbourg, CNRS, 23 Rue du Loess, 67037 Strasbourg, France*
(Received 29 April 1996; revised manuscript received 19 July 1996)

Giant magnetoresistive Co-Ag granular films are prepared by molecular beam epitaxy at three different temperatures with cobalt concentrations ranging from 30 to 80 at. %. The structural properties of these films are studied using a variety of diffraction techniques and real space probes. Magnetization and magnetotransport measurements are carried out at room temperature. Correlating the structural and magnetotransport properties reveals that the spin diffusion length strongly affects the amplitude of the giant magnetoresistance, which is otherwise dominated by the surface-to-volume ratio of the segregated magnetic precipitates. [S0163-1829(96)06441-7]

## I. INTRODUCTION

In recent years, considerable work has been carried out on the electrical transport properties of artificially layered structures. Giant magnetoresistance (GMR) was first measured in transition metal multilayers in which ferromagnetic (F) layers are coupled antiferromagnetically (AF) across a nonmagnetic (NM) spacer layer.[1,2] While the detailed mechanism of GMR remains incompletely resolved, it is clear that the phenomenon results from the spin-dependent scattering probability of electrons passing from a NM to a F region (interface scattering) and also within the F regions.[3,4] Electrons are more strongly scattered when their spins are misaligned with respect to the magnetization direction of the regions through which they are passing. In AF coupled multilayers, for which the F layers are aligned by an external magnetic field, the conduction electrons with spins antiparallel to the magnetization are strongly scattered at each F/NM interface, resulting in a high resistance for this spin channel. Those electrons whose spins are aligned with the magnetization do not experience this strong interfacial scattering and consequently the resistance for this spin channel is low. Since the two spin channels act in parallel, the low-resistance channel dominates the overall resistivity. When at low fields the F layers are AF aligned, none of the electron channels is aligned parallel to all of the F layers and they both experience strong scattering, leading to a high resistance.

The interest in GMR was subsequently strengthened by its discovery in granular films in which single-domain F grains are embedded in a NM metal matrix due to the immiscibility of the chosen materials.[5–7] The magnetic moments of the grains are aligned at high fields and misaligned at the coercive field leading to GMR in exact analogy to GMR in multilayers. This observation demonstrated that a layered structure is not a necessary condition for GMR, but a potential feature of any system containing F regions whose relative magnetic orientation may be externally manipulated.[8]

In granular films, the GMR depends even more critically on the film structure than in multilayers. However, because of the difficulties of controlling the structural characteristics of such inhomogeneous material, only a few detailed structural studies have been undertaken,[9–11] and they show a wide variation in behavior between nominally identical samples. Considering the current theory of GMR,[3,4] it is clear that this phenomenon depends upon a large number of magnetic and transport parameters such as the coercive and saturation fields, the total magnetization, the blocking temperature, and the spin diffusion length. In turn, these parameters are highly sensitive to the structure of the material. In the study of single-crystal magnetic films, these structural properties are well determined. By contrast, in granular materials, not only is sample growth more complex, but the microstructural texture can be varied over a wide range during deposition and through post-deposition treatments. It is one of the exciting aspects of engineering granular materials that subtle structural variations in many cases have dramatic effects on the parameters which control the magnetotransport. Thus it is possible to produce an enormous variety of novel magnetic systems with unusual properties. However, this versatility is a double-edged sword in the case where parameter control is less than total or where the effect of the various treatments is not fully understood. This can give rise to what appears in many cases to be a confusing lack of reproducibility from laboratory to laboratory and even from sample to sample in the same preparation batch.

In this paper we seek to fill a serious gap in the literature

 

by conducting a carefully controlled investigation into the microstructure generated by varying the growth temperature and the chemical composition. We then correlate the structural properties of the as-deposited films with the resultant transport characteristics. For this purpose, we prepared three series of epitaxial Co-Ag granular films by molecular beam epitaxy (MBE) as described in Sec. II. We have chosen Co-Ag since the efficiency of the scattering is most effective for this material combination giving rise to a large GMR amplitude. Section III of this article is devoted to the structural characterization using *in* and *ex situ* diffraction techniques and real space probes. Results for the magnetization and magnetotransport properties are presented in Sec. IV. Finally, we give a comprehensive picture of the relationship between structural and transport properties in granular systems in Sec. V, emphasizing the role of the spin diffusion length.

## II. EXPERIMENTAL PROCEDURE

Co-Ag films were deposited by molecular beam epitaxy at three different temperatures: 0 °C [low temperature (LT)], 300 °C [medium temperature (MT)], and 450 °C [high temperature (HT)] onto mica substrates. A 150-Å-thick epitaxial Ru film grown at 700 °C was used as a buffer layer onto which between 350 and 800 Å of Co and Ag were coevaporated and protected by a 30-Å-thick Ru capping layer. At each deposition temperature, the composition of the Co-Ag granular films was varied from 0 to 80 at. % of Co. Reflection high-energy electron diffraction (RHEED) was carried out during growth of the films.

After removing the samples from the UHV chamber, their structural characteristics were further investigated using x-ray diffraction techniques, both in-plane and cross-section transmission electron microscopy (TEM) and atomic force microscopy (AFM). The magnetic properties were measured at room temperature with an alternating gradient force magnetometer (AGFM). Magnetoresistance measurements were made using a four-point probe with the field parallel and perpendicular to the film plane and, in both cases, the current in the film plane. Because of the sharp drop in resistance of the Ru buffer layer at low temperature, only room temperature magnetoresistance measurements will be reported here. A parallel experiment is underway using Pt as the buffer layer for which the variation of the magnetoresistance with temperature will be studied in detail.

## III. STRUCTURAL PROPERTIES

In this section, the degree of phase segregation and the spatial extent of regions containing different chemical compositions in the Co-Ag films will be investigated.

### A. RHEED

Figures 1(a) and 1(b) show the RHEED patterns for a completed 150-Å-thick Ru buffer layer along the two characteristic azimuthal directions $[10\bar{1}0]$ and $[11\bar{2}0]$ of a close-packed hexagonal (0001) surface structure. The thin elongated RHEED streaks indicate long-range crystalline order of the Ru layer surface and a high degree of planarity. In the following, these patterns have been used for calibration of the lattice spacings, assuming that the Ru in-plane lattice parameter has relaxed to its bulk value of 2.71 Å.

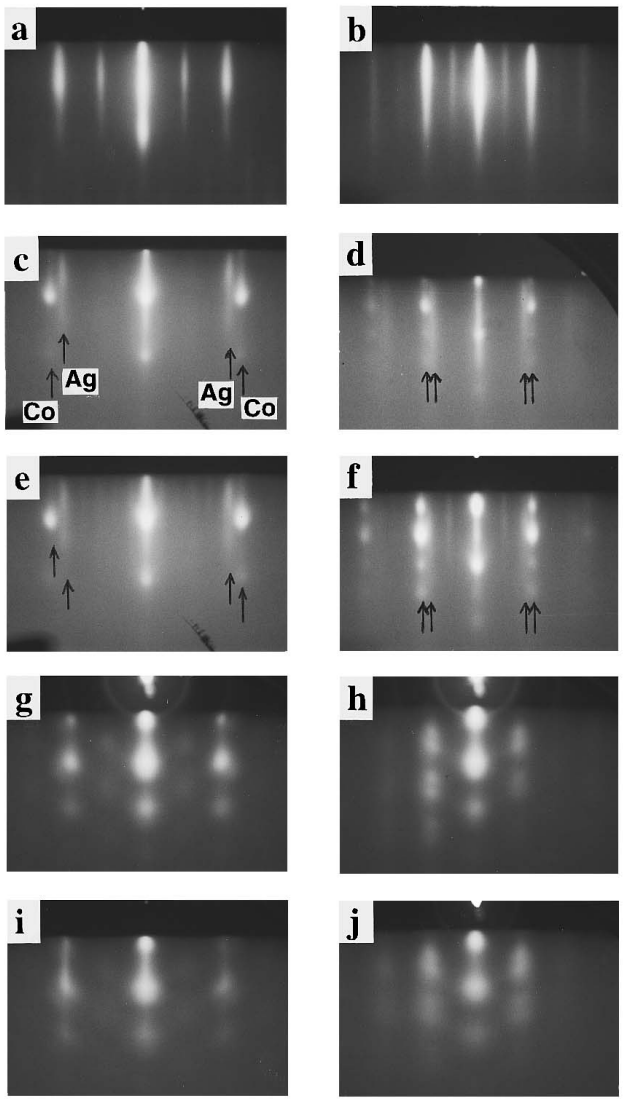


FIG. 1. Pairs of RHEED patterns observed during growth for Co-Ag films on a Ru buffer along two azimuths $[10\bar{1}0]$ (left hand column) and $[11\bar{2}0]$ (right hand column). In (c)–(f) the separate Co (outer) and Ag (inner) streaks are marked by arrows: (a) and (b) completed 150-Å-thick Ru buffer layer on mica, (c) and (d) 60 Å $Co_{43}Ag_{57}$ deposited at HT (450 °C), (e) and (f) 380 Å $Co_{43}Ag_{57}$ at HT, (g) and (h) 60 Å $Co_{43}Ag_{57}$ deposited at LT (0 °C), and (i) and (j) 380 Å $Co_{43}Ag_{57}$ at LT.

Figures 1(c)–1(f) show the RHEED patterns observed during the growth of a $Co_{43}Ag_{57}$ granular film at HT. There are now separate streaks representing the Co and Ag lattices (indicated by the arrows on the figure). The inner streaks derive from the Ag which has a larger nearest-neighbor distance in the hexagonal plane than the Co, the latter giving rise to the outer streaks. The Ag streak is very narrow, and spottiness is not observed even for thicknesses above 400 Å indicating the high crystalline quality of Ag. In contrast, the spotty Co streaks indicate three-dimensional-type growth. The Ag lattice parameter is found to be independent of the film thickness and close to the value for a pure Ag film, while that of the Co relaxes progressively from the Ru value

to the Co bulk value over the first 20 Å.[11,12] This is evidence of complete Ag and Co segregation as will be confirmed by x-ray and TEM measurements presented below.

For deposition at LT, epitaxy of the Co-Ag film with the Ru is retained for thicknesses up to 800 Å as seen from the symmetry of the RHEED patterns. However, it can be seen from Figs. 1(g) to 1(j) for a $Co_{43}Ag_{57}$ sample that at LT separate RHEED streaks from the Co and Ag lattices are not apparent and instead they are diffuse and spotty at 40 Å thickness and become increasingly so as the thickness increases. As this is in contrast to the growth of a pure Ag film on Ru buffer at the same temperature (LT), we conclude that adding Co induces crystalline disorder which increases with increasing film thickness. This suggests that the Co is homogeneously distributed in the film which results in the formation of small and slightly disoriented crystallites as will be confirmed by TEM. Thus we can conclude that the segregation is enhanced and hence the overall crystalline structure tends to improve as the growth temperature increases.

### B. X-ray diffraction

Reflectivity measurements were made in the $\theta/2\theta$ geometry to scan reciprocal space perpendicular to the film plane. We performed only high-angle scans around the first-order Bragg peak since the curvature of the mica (some few tenths of a degree) and the presence of steps due to the cleavage planes preclude small-angle reflectivity studies. Analysis of high-angle scans yields information on the average perpendicular lattice spacing $d$ (deduced from the position of the main Bragg peak) and the structural coherence length along the growth direction [deduced from its full width at half maximum (FWHM)]. The location of the Bragg peak compared to the positions found for the pure constituents provides an indication of the chemical composition.

Figures 2 and 3 show $\theta/2\theta$ scans for Co-Ag films of varying composition prepared at HT and LT, respectively. In both figures, the dashed lines correspond to the $2\theta$ angles expected for diffraction from bulk single crystals. The sharp peaks close to 63° and 70° originate from the mica substrates. The 150-Å-thick Ru buffer layer gives rise to the (0002) diffraction peak at 64.7°. The intensity of each spectra is normalized with respect to this Ru peak height. The peak at approximately 58.5° can be identified with the Ag(111) diffraction peak. Its intensity decreases as the Co content in the film increases. At HT the Ag peak remains visible for all concentrations (Fig. 2); however, at LT it has virtually disappeared for 50 at. % Co (Fig. 3). At MT, Ag can be detected up to a Co concentration of 70 at. %. The peak at 68.5°, which arises from hcp Co, is clearly visible only above 40 at. % Co at HT, 70 at. % at MT, and 86 at. % at LT. In addition to the fact that the diffracted intensity increases if the Co-Ag film contains a larger fraction of the corresponding metal, the evolution of the intensities clearly indicates that segregation is enhanced as the growth temperature increases and hence the crystalline structure of regions containing either Ag or Co improves. This is in agreement with the separate Co and Ag RHEED streaks which we observed for 57 at. % Co at HT, but not at LT. Also, the rapid decrease of intensity for the Ag x-ray peak from a pure Ag film to a $Co_{30}Ag_{70}$ film confirms the conclusion drawn from the RHEED study that adding Co at LT induces disorder.

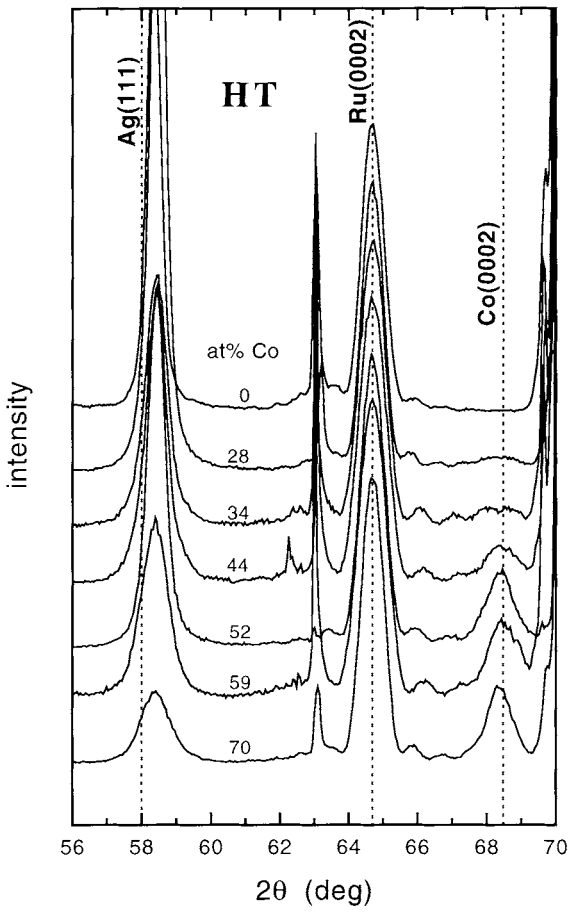


FIG. 2. X-ray $\theta/2\theta$ scans for Co-Ag granular films deposited at high temperature (450 °C) for Co concentrations ranging from 0 to 70 at. %. The dashed lines indicate the diffraction angles expected for bulk material.

However, even at 450 °C and high Co concentrations, the Co x-ray peak is very weak and relatively broad in comparison with the Ag peak. This is not in contradiction with the RHEED results since the instrumental coherence length in x-ray diffraction is considerably larger than for RHEED. The fact that the Ag peak remains strong for only 20 at. % of Ag in the film, but that no x-ray diffraction peak is visible for 20 at. % of Co, indicates the importance of atomic mobilities (Co atoms are less mobile than Ag atoms) for the formation of coherent crystalline regions.

The positions of the Ag(111) diffraction peaks are shifted towards higher angles with respect to the bulk value for fcc-Ag, indicating that the epitaxial film is contracted. This is the case even for pure Ag films grown at either HT or LT (top curve in Figs. 2 and 3, respectively). For Co-Ag films coevaporated at MT and HT, the interplanar lattice spacing $d_{111}$ remains approximately constant at the value of the pure Ag film. At LT, $d_{111}$ is further reduced in the range of Co concentrations between 30 and 43 at. %, which suggests that the two metals do not segregate but form a metastable Co-Ag phase consisting of small Co clusters embedded in a distorted fcc Ag matrix, resulting in a reduced average lattice spacing. This agrees well with the diffuse streaks observed in RHEED.

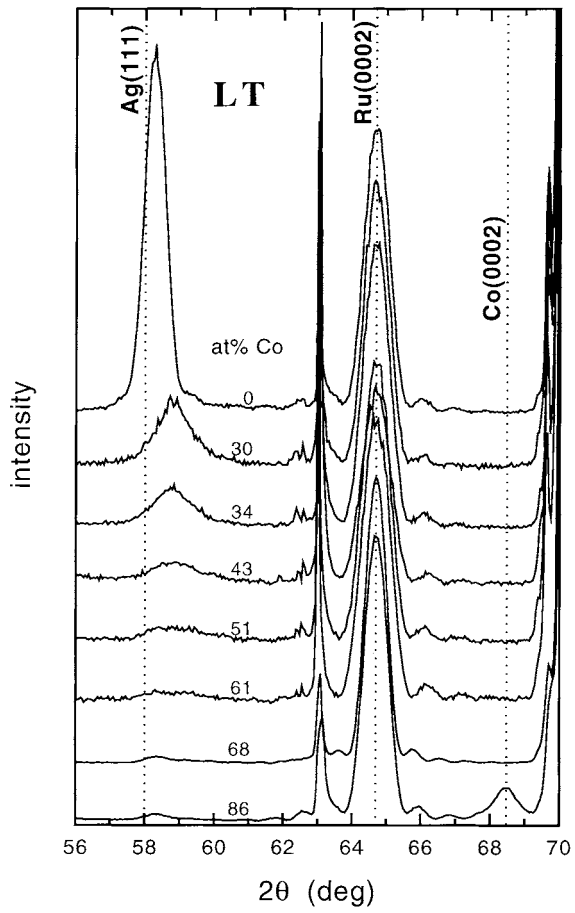


FIG. 3. X-ray $\theta/2\theta$ scans for Co-Ag granular films deposited at low temperature (0 °C) for Co concentrations ranging from 0 to 86 at. %. The dashed lines indicate the diffraction angles expected for bulk material.

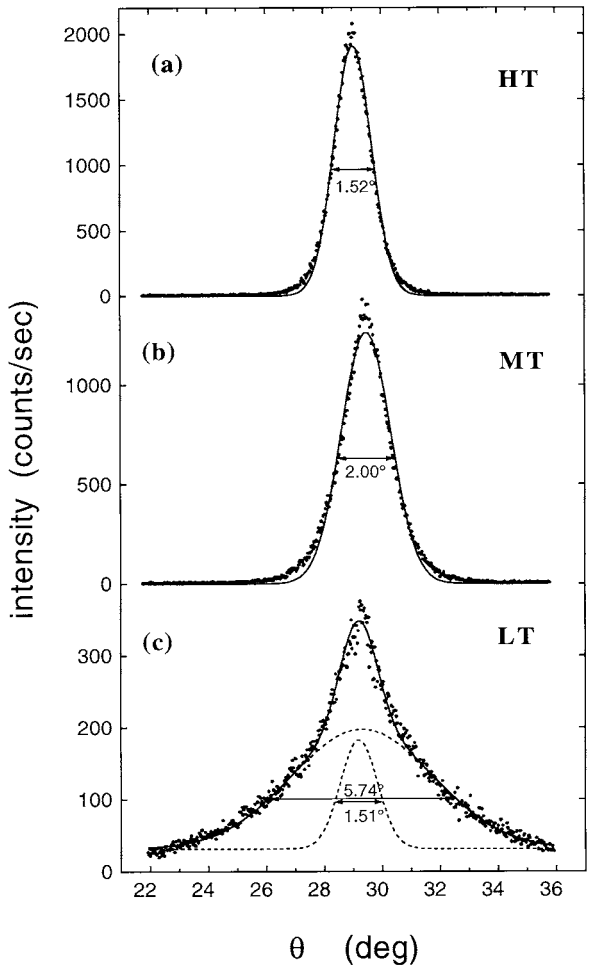


FIG. 4. X-ray rocking curves for $Co_{34}Ag_{66}$ films deposited at three different temperatures. The solid and dashed lines represent the Gaussians fitted to determine the peak width.

X-ray rocking curves across the out-of-plane Bragg peaks correspond to scanning the peaks parallel to the film plane and give information on the in-plane crystalline quality, such as the lateral structural coherence length and the mosaic spread within the epitaxial film. In general, this information is obtained by fitting an ensemble of Gaussians to the data.

In Fig. 4 rocking curves around the Ag(111) diffraction peak are shown for three Co-Ag films prepared at three different temperatures with a concentration of 34 at. % Co. For the HT samples, the shape of the rocking curves can be approximated by a single Gaussian [solid line in Fig. 4(a)]. The FWHM of this narrow peak, which derives from regions of well crystallized Ag, shows little variation with Co concentration and is between 0.8° and 1.5°. Since the FWHM is about 1.2° for the peak which arises from the Ru buffer layer, the small value found for Ag implies that no degradation of the lateral crystalline quality occurs over the several hundreds of Å thickness of the Co-Ag film. This is in agreement with the RHEED observations where two well-defined streaks for Co and Ag were found across the entire film thickness.

In contrast; for samples prepared at LT, for which the Co peak cannot be observed; the rocking curves around the Ag(111) diffraction peak can be decomposed into two contributions for all concentrations [dashed lines in Fig. 4(c)]: One is narrow (between 0.7° and 2.2°), and the other is much broader (between 4.9° and 7.2°) and of considerably higher integrated intensity. The narrow contribution, which derives from regions of well-crystallized Ag as in the case of HT samples, can be observed in the rocking curves even for samples with diffuse RHEED patterns. The broad contribution represents a large volume assembly of less well-oriented metastable crystallites containing both Co and Ag whose value of $d_{111}$ is intermediate between the values for bulk Ag and Co as indicated by the shift of the Ag(111) diffraction peak in the $\theta/2\theta$ spectrum.

The fact that the full peak height and the tail of the rocking curves at MT and HT cannot be fitted well with a single Gaussian [Figs. 4(a) and 4(b)] indicates that even in samples grown at elevated temperatures a small second contribution to the intensity is present which arises from these metastable Co-Ag crystallites. This has a significant influence on the spin diffusion length as discussed in Sec. V.

### C. Transmission electron microscopy and atomic force microscopy

While electron and x-ray diffraction provide a global view on the structural properties of the granular films, analyzing

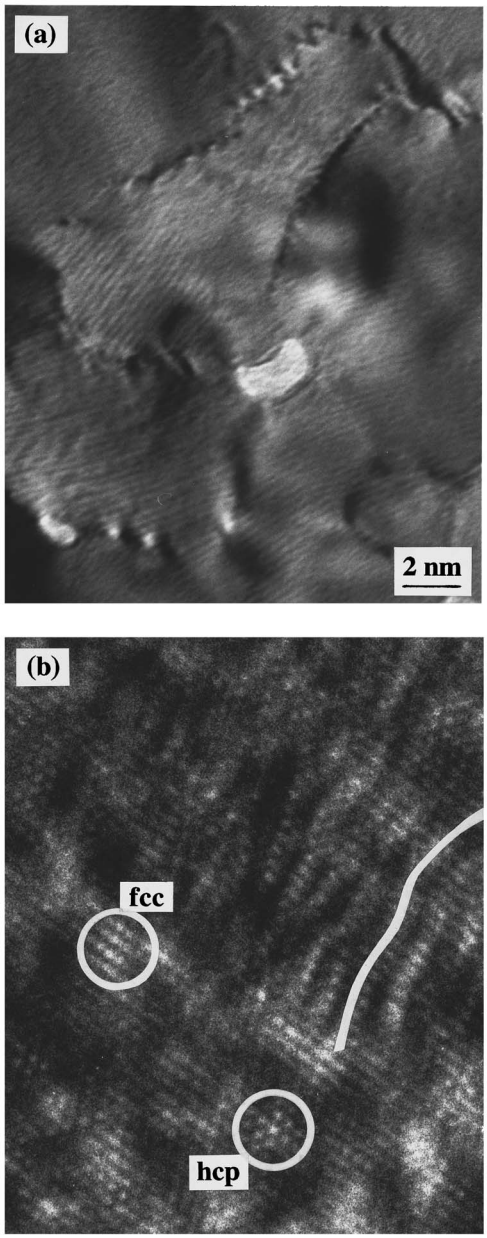


FIG. 5. (a) Plan view and (b) cross section transmission electron microscopy (TEM) images of a $Co_{43}Ag_{57}$ film deposited at LT.

the local atomic structure from plan view and cross section electron micrographs, together with information from the local chemical probe energy dispersive x-ray analysis (EDAX), allows us to develop a detailed picture of the formation of Co clusters, their atomic structure, and their spatial distribution as a function of the growth temperatures. We have chosen samples of a medium Co content (43 at. %), in order to see the onset of the grain formation, but not to enter the regime of percolation.

The plan view electron diffraction patterns for a LT $Co_{43}Ag_{57}$ granular film revealed two different regions within the sample where in (i) the Co and Ag are segregated and both in the fcc phase and in (ii) only the fcc Ag phase is well defined. Therefore, if regions of hcp Co are present, they must be smaller than 100 Å.[13]

The plan view TEM images show approximately spherical inclusions with a diameter of the order of 50 Å [Fig. 5(a)]. These inclusions are identified from the strong contrast around them due to dislocations or elastic strain which are present to accommodate the lattice mismatch between the inclusions and the surrounding matrix. The ''torn'' lines are directly related to the dislocations. EDAX measurements reveal that these inclusions are either rich (more than 80 at. %) in Co or rich in Ag, while the surrounding matrix has an average Co content of 45 at. %.

Two structural features along the growth direction are revealed by the cross section TEM image shown in Fig. 5(b): (i) Analyzing the stacking sequence of the atomic planes reveals that the matrix is primarily in the fcc structure (ABCABC stacking) in agreement with the diffraction patterns. In addition, small (10–20 atoms) clusters of hcp structure (ABAB stacking) are found which we assume to be Co and which are too small to be detected by diffraction. [Regions where the stacking sequence can be clearly identified are enclosed by circles in Fig. 5(b).] It is estimated that these clusters contain about 8 at. % of the total Co in the film so that the remaining 35 at. % of Co is in the fcc phase in the matrix. (ii) The dark and light contrast running across the figure is caused by dislocations perpendicular to the visible (111) planes. This contrast gives the appearance of waves across the sample [traced by a white line in Fig. 5(b)] which are broken up into structures about 20 Å long and a few atomic planes wide approximately parallel to the Ru buffer layer. These waves may be evidence of a compositional variation on a length scale of 20–30 Å. In conclusion, some phase segregation is observed both on a large scale (inclusions) and a small scale (hcp clusters); however, large regions of pure metal were not found.

The plan view electron diffraction patterns for a HT Co-Ag granular film containing 43 at. % Co show clear evidence of fcc Ag and hcp Co in contrast to the LT sample. With the incident beam along the [0001] axis of the hcp Ru and the [111] axis of the fcc Ag, any fcc Co diffraction spot, if present, would be superimposed by $\langle \bar{2}1\bar{1}0 \rangle$ hcp spots, and hence no assumption can be made on the existence of fcc-Co. In contrast to the LT sample, there is little contrast in the plan view micrograph providing evidence for the improved crystallinity for films grown at HT.

Cross section TEM enables us to distinguish between different regions within the sample. Adjacent to the Ru buffer layer, regions of pure and well-crystallized Ag [Fig. 6(a)] or Co [Fig. 6(b)] are observed. In the case of Co, these regions are approximately 30 Å thick. On top of the Co and up to the total film thickness of approximately 350 Å, a mixture of Co and Ag is found which is either well segregated in clusters varying in size from 100–200 Å [Fig. 6(c)] or in a Co-Ag metastable phase [Fig. 6(d)] which has the approximate lattice spacing of a Ag film. These images indicate that Co and Ag are not fully segregated even at HT. In contrast, the pure Ag regions adjacent to the Ru buffer [Fig. 6(a)] extend across the total film thickness which is only 150 Å in these regions.

These cross section TEM results correlate with the AFM image in Fig. 7(a) for a $Co_{34}Ag_{66}$ film deposited at HT which shows raised areas of 1 $\mu$m diameter separated by 0.2-$\mu$m-wide gaps. The AFM image recorded for a film of the same composition but prepared at LT [Fig. 7(b)] shows some surface roughness, but on a much smaller lateral length scale in

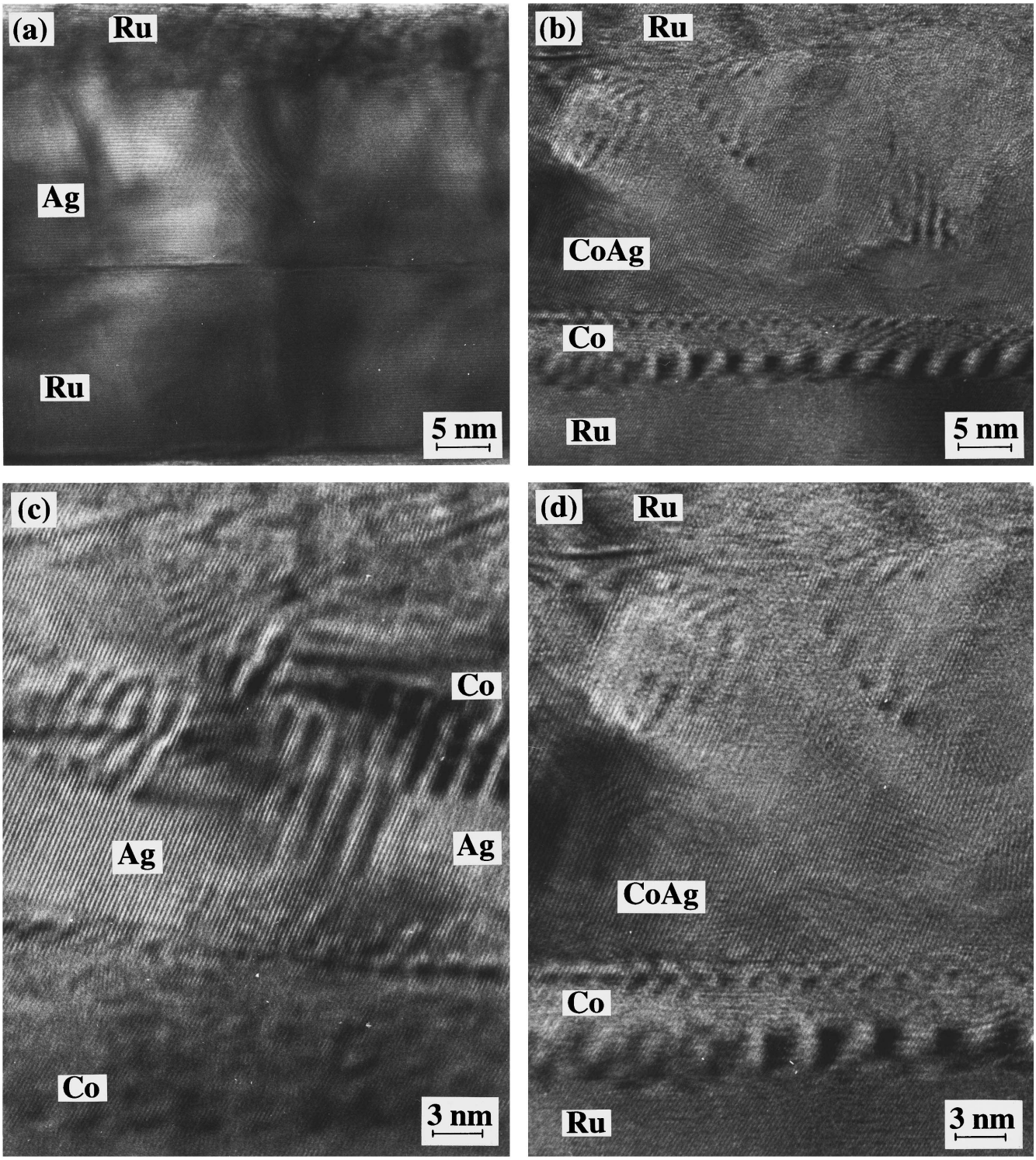


FIG. 6. Cross-section TEM images for a $Co_{43}Ag_{57}$ granular film prepared at HT. (a) and (b) show regions of different total thickness including the 150 Å Ru buffer and the 30 Å Ru cap layer for the same film. (a) Shows a thin (150 Å) region of pure (111) Ag planes with no dislocations or strains. The thick (250 Å) region in (b) contains areas of dislocations. From the period of these dislocations, the lattice mismatch between the adjacent regions can be calculated (Ref. 13) which identifies a pure Co region at the interface with the Ru-buffer layer and a mixed Co-Ag region above. Enlarged images obtained from this mixed region at two different sites are shown in (c) and (d). Counting the atomic planes at the dislocations reveals that Co and Ag are segregated in (c) while EDAX gives evidence for a homogeneous mixture in (d).

agreement with observations made by cross section TEM. We find that the surface of a pure Ag film grown at HT (not shown here) contains even larger raised areas if compared with Fig. 7(a). In the case of a pure LT-Ag film, the observed roughness is very similar to the film with 34 at. % of Co shown in Fig. 7(b), but as the Co concentration increases further, the size of the topographical features decreases. This suggests that the surface topography is determined predomi-

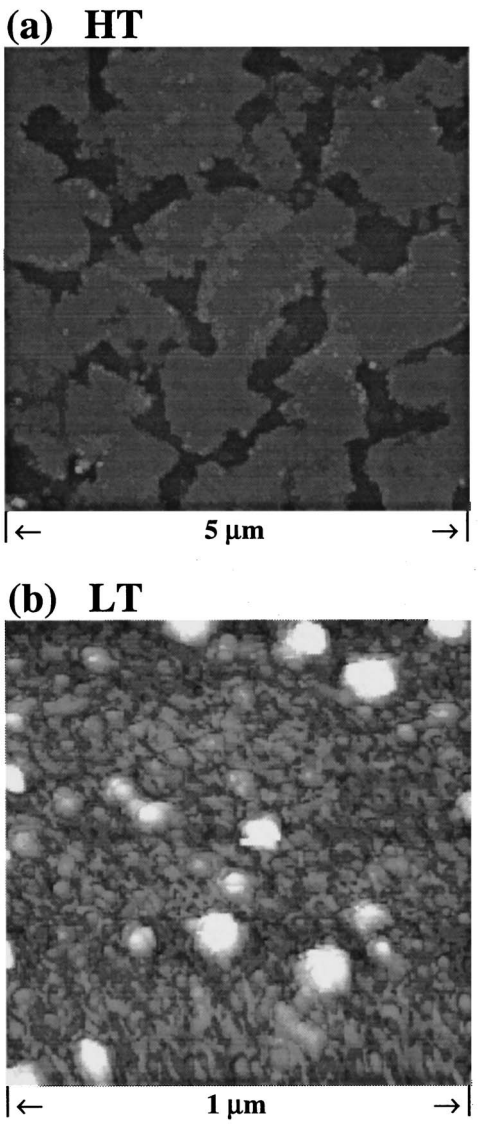


FIG. 7. AFM images of $Co_{34}Ag_{66}$ films deposited at HT and LT.

nantly by the amount and the mobility of the Ag since islands become increasingly small as either the growth temperature is reduced or the Co concentration is increased.

TEM results for samples prepared at MT are intermediate between the LT and HT samples, but show features more similar to the HT ones.[13]

### D. Discussion and summary of the film structure

It is known that the magnetotransport properties of granular metal films can be altered through thermal treatment.[14,16] The observed changes are commonly attributed to an increase of the size of the magnetic precipitates. Our results on the structural properties of as-grown epitaxial Co-Ag films clearly demonstrate that the structure of granular films is much more complex. A variety of phases are found to coexist in all samples; however, certain trends were observed, notably that phase segregation and long-range crystalline order increase as the growth temperature increases. This can be understood from the enhanced mobility of the atoms on a substrate surface held at an elevated temperature.

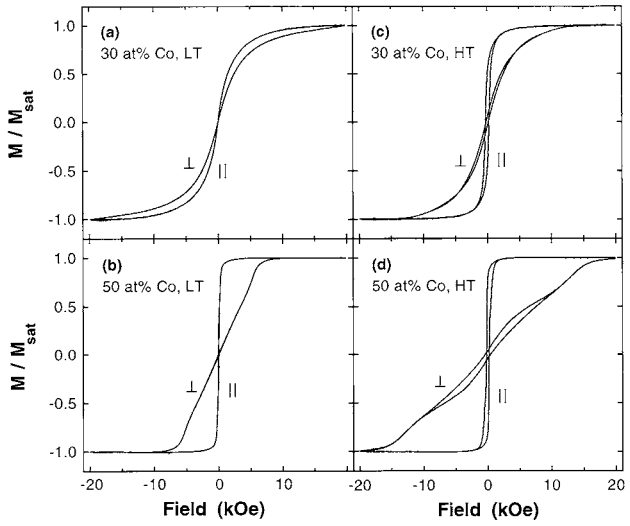


FIG. 8. In- and out-of-plane room temperature magnetization curves for $Co_{30}Ag_{70}$ and $Co_{50}Ag_{50}$ films prepared at LT and HT, respectively. Note that the large hysteresis and the undulating shape of the perpendicular magnetization curve in (d) is an artifact which arises from torque exerted onto the sample when it is not placed entirely within the homogeneous field region of the AGFM.

In the LT samples, phase segregation is observed only on a very small scale, while extended regions consist of Co present in the form of small clusters (or possibly single atoms) embedded in the Ag matrix. The process of percolation sets in as the Co concentration increases, however, these Co-rich regions do not crystallize coherently over a sufficient length scale to give rise to diffraction peaks in RHEED or x-ray $\theta/2\theta$ scans. The surface topography of these films [AFM, Fig. 7(b)] contains only small scale variations of the film thickness.

If we refer to previous work on Co/Ag multilayers, we can understand the structure of our HT samples. It has been observed that the lattice parameter of Co grown on Ag relaxes over a few atomic layers from the value of the pure Ag film to bulk Co,[17] whereas Ag grown on Co relaxes immediately to its bulk value.[18] With this in mind, it is apparent from the sharpness of our RHEED streaks for samples prepared at HT [Figs. 1(c) to 1(f)] and also from the constancy of the Ag lattice parameters with film thickness that there is only restricted growth of Co on top of Ag. Hence, during the early stages of metal deposition, phase segregation leads to the formation of extended regions containing either Ag or Co adjacent to the Ru buffer [TEM, Figs. 6(a) and 6(b)]. As the coevaporation proceeds, some Ag sticks to the Co, giving rise to the raised regions containing both Co and Ag which were identified with TEM and AFM [Fig. 7(a)].

## IV. MAGNETIC AND MAGNETOTRANSPORT PROPERTIES

### A. Magnetization

Magnetization curves for the coevaporated epitaxial Co-Ag films were recorded at room temperature in a magnetic field up to 20 kOe with the field oriented parallel and perpendicular to the film plane. Selected magnetization curves are shown in Fig. 8.

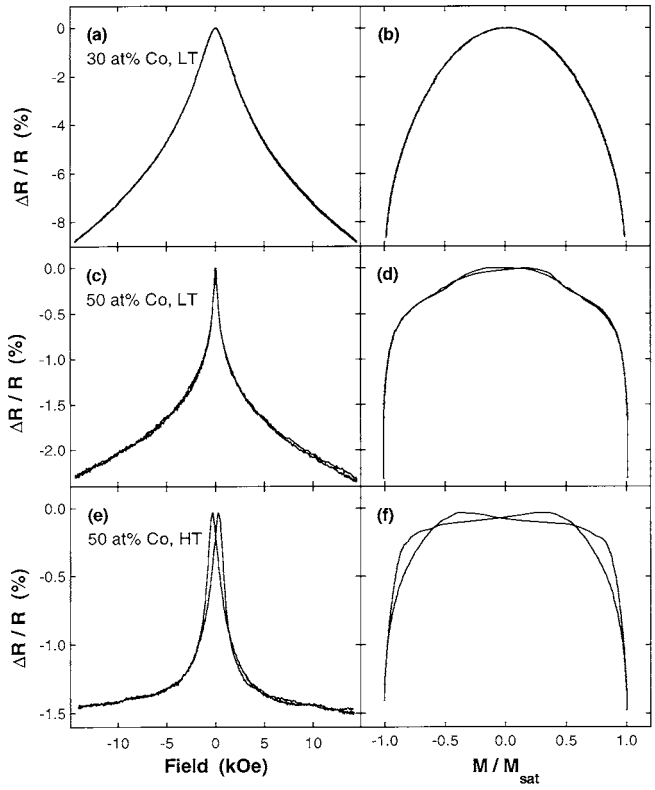


FIG. 9. Correlation of the in-plane GMR and magnetization for a $Co_{30}Ag_{70}$ and a $Co_{50}Ag_{50}$ film prepared at LT and HT.

Only samples prepared at LT with less than 40 at. % Co show pure superparamagnetic behavior for both field orientations [Fig. 8(a)]. This is consistent with the existence of small single-domain magnetic regions which we observed in the TEM images. Above 50 at. %, the separation between single-domain magnetic regions decreases, leading to interparticle exchange coupling and hysteresis[19] [Fig. 8(b)]. The coercive field $H_c$ increases gradually as the Co concentration increases reaching about 100 Oe for 80 at. % Co. Films prepared at MT and HT show predominantly ferromagnetic behavior [Fig. 8(c) and 8(d)] with $H_c$ of the order of 200 Oe. As the Co concentration exceeds 50 at. % in the HT films, the coercive field values begin to decrease due to the onset of domain wall motion in the relatively large pure Co regions. All samples show magnetic anisotropy with the hard axis perpendicular to the film plane. For all those films which show hysteresis, the in-plane saturation fields $H_{sat}$ are similar and in the range of 500 Oe. Out-of-plane $H_{sat}$ is between 6 and 10 kOe for LT samples and higher for films deposited at elevated temperatures. The tendency that out-of-plane $H_{sat}$ increases with increasing Co reflects the increasing importance of shape anisotropy as the film approaches the limit of a pure thin Co film.

### B. Giant magnetoresistance

In the left-hand column of Fig. 9, magnetoresistance curves are shown for three Co-Ag films for which the corresponding magnetization loops are displayed in Figs. 8(a), 8(b), and 8(d), respectively. We selected curves typical for a predominantly superparamagnetic [Fig. 9(a)] and predominantly ferromagnetic films [Figs. 9(c) and 9(e)]. In all cases,

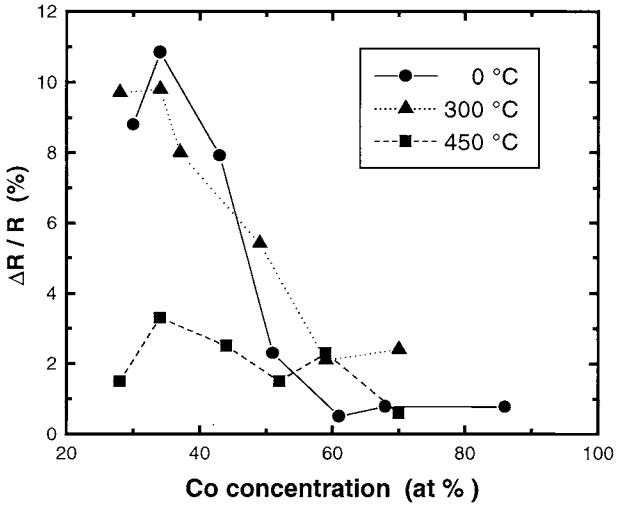


FIG. 10. Variation of the peak GMR measured at room temperature as a function of Co concentration for three deposition temperatures.

the maxima of the GMR curves coincide with the coercive fields (compare with Fig. 8), since maximum magnetic disorder exists at $H_c$. However, the MR did not saturate for any of the samples prepared for this study in the highest field available to us of 14 kOe, in contrast to the magnetization, which saturated in-plane at fields ranging from a few 100 Oe to 5 kOe. Indeed, transport measurements have an enhanced sensitivity to small magnetic misalignments over magnetometry with respect to probing magnetization states. The curves in the right-hand column of Fig. 9, which display the correlation between the field dependence of the magnetization process and the GMR, will be discussed in the next section.

## V. DISCUSSION: CORRELATION OF THE GIANT MAGNETORESISTANCE BEHAVIOR WITH THE FILM STRUCTURE

Heterogeneous alloys are complex systems, and there are many factors which affect both the maximum value of GMR and its variation with applied field. We shall now consider the different scattering mechanisms which control the shape of the magnetoresistance curves (Fig. 9) and the magnitude of the GMR (Fig. 10). We will then examine how the structure of the film affects these mechanisms and identify examples from our data set for which a particular mechanism dominates. As is evident from the structural data presented in this article, Co-Ag granular films are far from idealized systems which might contain well-crystallized metallic Co spheres embedded in a pure Ag matrix. For the purposes of this discussion, we shall therefore refer to the active magnetic regions as magnetic grains. These grains may be a collection of smaller correlated regions which magnetize cooperatively due to strong ferromagnetic interactions between them or they may be metastable Co-Ag regions with a Co content large enough to induce magnetic order. Where the actual composition or structure of the grains is important this will be expanded upon.

As outlined in the Introduction, the spin-dependent interface scattering mechanism depends on the relative orientation of the magnetic grains and hence the GMR is expected

to be proportional to $(M/M_{sat})^2$ for noninteracting magnetic single-domain grains embedded in a conducting matrix.[20] This would yield a parabolic curve if the GMR is plotted versus the normalized magnetization. It can be seen from the plots in the right-hand column of Fig. 9 that this is only the case for the film prepared at LT with 30 at. % of Co. This is consistent with the existence of small independent unblocked magnetic grains which give rise to the superparamagnetic behavior shown in Fig. 8(a).[19] For higher Co concentrations or elevated growth temperatures, the magnetization reversal no longer proceeds through the rotation of independent magnetic grains, as deduced from the magnetization curves in the previous section. However, the mechanism of reversal is different for the two films shown in Figs. 9(c) and 9(e). In the former case, ferromagnetic interactions induce a collective rotation of the single-domain grains, which strongly affects the net magnetization at small external fields, but keeps the relative orientation of the magnetic grains fixed and hence the GMR does not change. This gives rise to the flat top of the curve in Fig. 9(d). Beyond a certain field strength the relative orientations change and GMR is observed. For the HT sample containing 50 at. % of Co, a flat-topped parabola also arises because there is little change of the GMR at small external fields, but a large change of the net magnetization. However, in this case the reversal mechanism proceeds via the formation of magnetic domains within the grains, which results in little change in the magnetoresistance.

### A. Scattering mechanisms

The actual cause of GMR is the spin-dependent scattering which can be considered to occur either within the magnetic grain or at the F/NM interfaces. These two mechanisms imply a different dependence of the GMR with grain size. In the case of interface scattering, the ratio of surface area to volume of the Co grains should be increased for high GMR, i.e., small grains will be more efficient spin-dependent scatterers. For bulk scattering we can define a spin-filtering length which corresponds to the length of time the electron must spend inside the grain for the spin information to be coded upon it. However, this simple dependence on grain size is further complicated by the fact that an increase in grain size is usually accompanied by a change of the separation between grains and by the additional action of a spin depolarization mechanism whose efficiency also increases with grain size. As described below, these two mechanisms affect the spin diffusion length and hence the GMR. The combination of these effects produces an *optimum* grain size for the GMR.

### B. Spin diffusion length

For GMR to occur, the spin orientation of an electron traveling between magnetic grains must be conserved; i.e., it is vital that the spin information coded onto the conduction electron in one magnetic region survives until it reaches the next one. The spin orientation can be altered by processes during which the electron momentum is conserved, but its spin is flipped.[21] The distance over which the electron travels before its spin is flipped is defined as the spin diffusion length. The spin diffusion length is the determining length scale for granular GMR systems. Any mechanism that acts to reduce the ratio of the spin diffusion length to the separation of the magnetic regions or acts in any way to mix the spin channels will therefore have a detrimental effect on the GMR.

(i) *Separation of the magnetic grains.* For two samples with identical matrices, but different separations between the magnetic grains, there are two mechanisms controlling the magnitude of the GMR. (a) The sample with the greater separation between grains will have a lower GMR due to spin flip scattering in the matrix [see point (ii) below] and (b) the greater separation will act to reduce ferromagnetic interactions between grains tending to increase the GMR.

(a) For our series of samples grown at MT and HT, the quality of the matrix changes little across the range of compositions studied as evidenced by the x-ray diffraction spectra and the RHEED patterns. We can therefore expect the spin diffusion length to be similar. For two films with the same Co concentration, but prepared at either 300 or 450 °C, the grains are larger and separated further at HT and as a result the GMR is lower. This is the main origin for the small GMR in the HT Co-Ag granular films in Fig. 10. The highest value for the GMR would be expected for films deposited at LT since the surface-to-volume ratio of the grains is even larger and the separation between grains is smaller; however, the spin diffusion length is strongly reduced as we shall see in the following section.

(b) Interparticle coupling will change as the separation is increased, reducing ferromagnetic interactions which would otherwise be detrimental to the GMR. However, at low temperatures and compositions we can see from the parabolic shape of the curve in Fig. 9(a) that there are no ferromagnetic interactions for samples grown at LT until the Co composition exceeds 50%. This contrasts with the HT samples for which ferromagnetic interactions are apparent.

(ii) *Paramagnetic impurities.* The primary mechanism within the matrix causing spin channel mixing and hence a reduction of the spin diffusion length is spin flip scattering at paramagnetic impurities. It has been calculated that the spin diffusion length can be reduced by as much as an order of magnitude for only 8% Co impurities in a Ag matrix.[21] It is clear from the structural analysis of our samples that the Ag matrix is severely distorted in the LT films and there is clear evidence for the presence of Co impurities in the Ag matrix. In contrast, the x-ray studies show nearly pure Ag matrices for the MT and HT films which have therefore similar, relatively long, spin diffusion lengths. Hence the GMR is expected to be strongly reduced in the Co-Ag films grown at 0 °C with respect to MT and HT. In Fig. 10 we observe a similar magnitude of the GMR for LT and MT. This is because the surface-to-volume ratio and the separation of the magnetic grains discussed in point (i) would otherwise have given rise to a larger GMR for the LT films. The GMR has been strongly reduced due to the effect of the spin diffusion length and as a result has a similar magnitude as the GMR for films deposited at 300 °C.

At around 50 at. % of Co, the GMR for the MT and LT films drops due to the rapidly increasing grain size and ferromagnetic interactions of the magnetic grains at the onset of percolation. In addition, the matrix of the films grown at 0 °C becomes increasingly distorted as the Co concentration increases, which results in a decreasing spin diffusion length

due to impurity scattering. This effect accounts for the steeper decrease of the GMR around 50 at. % of Co for the LT with respect to the MT films as observed in Fig. 10.

(iii) *Jitterbug spin depolarization.* This is a carrier depolarization mechanism which mixes the spin channels[22] and hence reduces the spin diffusion length when adjacent magnetic regions are imperfectly aligned. The mixing occurs by virtue of the pseudo-Larmor precession of the carrier about the exchange fields within successive misaligned single-domain grains in its path. The effect of jitterbug spin depolarization is most pronounced at large external fields where it slows the approach to saturation of the GMR with respect to the magnetization. This is due to its high sensitivity to small magnetization misalignments, whereas these produce only imperceptibly small deviations of the net magnetization from saturation (compare Figs. 8 and 9). This effect is present even for HT samples [Fig. 9(e)] due to residual Co in the Ag matrix despite the strong segregation as indicated by the tails in the x-ray rocking curves [Fig. 4(a)]. The degree of precession also increases with the diameter of the grains. As the relative angle between the moments of a magnetic grain and the electron spin increases, the probability of scattering tends to 1.

## VI. SUMMARY

We have demonstrated the importance of the film structure in determining the magnetotransport properties of epitaxial granular Co-Ag films and, in particular, the effect of changes in the spin diffusion length. We have identified three mechanisms which tend to reduce the spin diffusion length and hence the GMR and presented examples from our experimental data for which one of these mechanisms dominates: (i) The large separation between magnetic grains is responsible for the overall small GMR in films deposited at HT, (ii) spin flip scattering from magnetic impurities is most pronounced for LT films, and (iii) the jitterbug spin depolarization gives rise to the tails of the GMR behavior at high external fields.

## ACKNOWLEDGMENTS

The authors gratefully acknowledge the support of the European Human Capital and Mobility program, the Alliance program between the Ministère des Affaires Etrangères and the British Council, and the EPSRC.

[1] M. N. Baibich, J. M. Broto, A. Fert, F. Nguyen Van Dau, F. Petroff, P. Etienne, G. Creuzet, A. Friederich, and J. Chazelas, Phys. Rev. Lett. **61**, 2472 (1988).

[2] G. Binasch, P. Grünberg, F. Saurenbach, and W. Zinn, Phys. Rev. B **39**, 4828 (1989).

[3] R. E. Camley and J. Barnas, Phys. Rev. Lett. **63**, 664 (1989).

[4] P. M. Levy, S. Zhang, and A. Fert, Phys. Rev. Lett. **65**, 1643 (1990); S. Zhang, P. M. Levy, and A. Fert, Phys. Rev. B **45**, 8689 (1992).

[5] A. E. Berkowitz, J. R. Mitchell, M. J. Carey, A. P. Young, S. Zhang, F. E. Spada, F. T. Parker, A. Hutten, and G. Thomas, Phys. Rev. Lett. **68**, 374 (1992).

[6] J. Q. Xiao, J. S. Jiang, and C. L. Chien, Phys. Rev. Lett. **68**, 3749 (1992).

[7] J. A. Barnard, A. Waknis, M. Tan, E. Haftek, M. R. Parker, and M. L. Watson, J. Magn. Magn. Mater. **114**, L230 (1992).

[8] B. Dieny, V. S. Speriosu, S. S. P. Parkin, B. Gurney, D. Wilhoit, and D. Mauri, Phys. Rev. B **43**, 1297 (1991).

[9] B. Dieny, S. R. Teixeira, B. Rodmaq, C. Cowache, S. Auffret, O. Redon, and J. Pierre, J. Magn. Magn. Mater. **130**, 197 (1994).

[10] S. S. P. Parkin, R. F. C. Farrow, T. A. Rabedeau, R. F. Marks, G. R. Harp, Q. Lam, C. Chappert, M. F. Toney, R. Savoy, and R. Geiss, Europhys. Lett. **22**, 455 (1993).

[11] A. Azizi, S. M. Thompson, K. Ounadjela, J. F. Gregg, P. Vennegues, A. Dinia, J. Arabski, and C. Fermon, J. Magn. Magn. Mater. **148**, 313 (1995).

[12] D. Muller, K. Ounadjela, P. Vennegues, V. Pierron Bohnes, A. Arbaoui, J. P. Jay, A. Dinia, and P. Panissod, J. Magn. Magn. Mater. **104**, 1873 (1992).

[13] A. Azizi, L. El Chahal, K. Ounadjela, J. P. Deville, S. M. Thompson, and J. F. Gregg, J. Appl. Phys. **79**, 6247 (1996).

[14] P. Crespo, A. Hernando, R. Yavari, O. Drbohlav, A. Garcia Escorial, J. Barandiarán, and I. Orúe, Phys. Rev. B **48**, 7134 (1993).

[15] J. Q. Wang and G. Xiao, Phys. Rev. B **49**, 3982 (1994).

[16] S. B. Slade, F. T. Parker, and A. E. Berkowitz, J. Appl. Phys. **75**, 6613 (1994).

[17] E. A. M. van Alphen, S. G. E. te Velthuis, H. A. M. de Gronckel, K. Kopinga, and W. J. M. de Jonge, Phys. Rev. B **49**, 17 336 (1994).

[18] K. Sakai and T. Kingetsu, J. Cryst. Growth **126**, 184 (1993).

[19] J. F. Gregg, S. M. Thompson, S. Dawson, K. Ounadjela, C. Staddon, J. Hamman, C. Fermon, and K. O'Grady, Phys. Rev. B **49**, 1064 (1994).

[20] J. Q. Xiao, J. S. Jiang, and C. L. Chien, Phys. Rev. B **46**, 9266 (1992).

[21] A. Fert, J. L. Duvail, and T. Valet, Phys. Rev. B **52**, 6513 (1995).

[22] G. A. Gehring, J. F. Gregg, S. M. Thompson, and M. L. Watson, J. Magn. Magn. Mater **140–144**, 501 (1995).